Theory of magnetically coupled type-II superconducting films

John R. Clem
Ames Laboratory-USAEC and Department of Physics, Iowa State University, Ames, Iowa 50010
(Received 13 August 1973)

The current-voltage characteristics of a magnetically coupled pair of infinite type-II superconducting films of finite thickness, separated by an insulating layer, are calculated. The main features of the time-averaged primary and secondary flux-flow voltages $\bar{V}_p$ and $\bar{V}_s$ versus the primary and secondary currents I_p and I_s are found to depend upon only five parameters: the primary and secondary critical depinning currents I_{pc} and I_{sc}, the primary and secondary flux-flow resistances R_p and R_s, and a coupling current I_0, which is proportional to the maximum coupling force exerted on a secondary fluxoid by the displaced primary-fluxoid lattice. Model calculations of the current-voltage characteristics are performed to illustrate predicted behavior under varying strengths of current, pinning, and coupling.

I. INTRODUCTION

Since the discovery by Giaever[1] that fluxoid motion in a primary superconducting film could induce fluxoid motion and an associated voltage in an adjacent secondary superconducting film, the theory of magnetically coupled superconducting films has undergone a relatively slow development. Probably the most important step towards such a theory was made by Cladis, Parks, and Daniels,[2] who stated the equations of motion for the primary and secondary fluxoids, ignoring pinning but including a periodic coupling force between a secondary fluxoid and the primary-fluxoid lattice. Their main result was to show qualitatively why slippage between the primary and secondary lattices should occur for sufficiently high fluxoid velocities. Because of strong pinning effects and associated instabilities in the specimens of most experiments to date, there has seemed to be little hope of obtaining good quantitative agreement with this theory.

As will be described in the following paper,[3] however, coupled granular-aluminum films, in which the pinning force can be made quite small, are almost ideal systems for the study of magnetic coupling. Experiments in these films show good qualitative agreement with some of the features of the Cladis-Parks-Daniels theory,[2] but point up the need for generalization of this theory, not only to include the effects of bulk pinning and applied currents in both the primary and the secondary, but also to make provisions for detailed quantitative comparisons between experimental and theoretical values of the maximum coupling force.

In this paper we shall discuss in Sec. II the origin of the periodic coupling energy, which is responsible for the primary-secondary coupling force. In Sec. III we shall derive equations of motion for the coupled system, including the effect of pinning and of currents in both films. The current-voltage characteristics that emerge from a solution of these equations are displayed for a variety of combinations of current, pinning, and coupling. In Sec. IV we shall discuss these results and outline some prospects for future theoretical and experimental work.

II. COUPLING ENERGY

Let us consider a pair of infinite type-II superconducting films parallel to the x-y plane. The lower film, called the primary, has thickness d_p and penetration depth λ_p and is separated by an insulating layer of thickness d_i from the upper film, called the secondary, which has thickness d_s and penetration depth λ_s. (The terms primary and secondary are used because a pair of magnetically coupled films may be regarded as a dc transformer.)

When a magnetic field is applied perpendicular to the films, singly quantized fluxoids are present in the two films. We assume that the energetically most favorable configuration of these fluxoids is a perfect triangular lattice of fluxoids in each film. The average flux density is $B = \varphi_0/A$, where $\varphi_0 = hc/2e$ and $A = \frac{1}{2}d^2\sqrt{3}$ is the area of the unit-cell parallelogram for the triangular lattice of nearest-neighbor distance d.

The Gibbs free energy is minimized when the primary-fluxoid lattice is in perfect registry directly below the secondary lattice. When the primary lattice is displaced from registry through the vector $\vec{s}$, the energy increases, primarily because the magnetic field energy and the kinetic energy of the supercurrents in the region between the films are higher in the displaced configuration than when in perfect registry. The increase in energy of interaction of a secondary fluxoid with the primary-fluxoid lattice is then $E_c(\vec{s})$, which we call the coupling energy. The coupling energy has the same periodicity as the primary-fluxoid lattice, $E_c(\vec{s}+\vec{l}) = E_c(\vec{s})$, where $\vec{l}$ is a fluxoid-lattice vector. Note that $E_c(0) = 0$ by definition.

When the current and field distributions are given to good approximation by the superposition of the

current and field contributions from individual fluxoids in the two films, it is convenient to write

$$E_c(\vec{s}) = \sum_{\vec{l}} v(\vec{l}, \vec{s}) \ . \tag{2.1}$$

Here $v(\vec{l}, \vec{s})$ is the change in interaction energy between a secondary fluxoid at the origin and a primary fluxoid whose initial and final displacements from the origin are $\vec{l}$ and $\vec{l}+\vec{s}$. The sum extends over all lattice vectors $\vec{l}$ in the primary. As shown in Ref. 4, it is possible to write

$$v(\vec{l}, \vec{s}) = (2\pi)^{-2} \int d^2q\, \tilde{v}(q) e^{i\vec{q}\cdot\vec{l}} (e^{i\vec{q}\cdot\vec{s}} - 1) \ , \tag{2.2}$$

where $\tilde{v}(q)$ is the two-dimensional Fourier transform of the primary-secondary-fluxoid-interaction energy and $\vec{q}$ is a wave vector perpendicular to the z axis. Combining Eqs. (2.1) and (2.2) and making use of

$$\sum_{\vec{l}} e^{i\vec{q}\cdot\vec{l}} = A^{-1}(2\pi)^2 \sum_{\vec{g}} \delta(\vec{q} - \vec{g}) \ , \tag{2.3}$$

where the sum is over all reciprocal-lattice vectors $\vec{g}$, we obtain

$$E_c(\vec{s}) = A^{-1} \sum_{\vec{g}}{}' \tilde{v}(g)(e^{i\vec{g}\cdot\vec{s}} - 1) \ . \tag{2.4}$$

The prime on the summation denotes omission of the term with $\vec{g} = 0$.

As will be shown in Ref. 4, $\tilde{v}(q)$ may be obtained with the help of the London model[5,6] for the primary and secondary fluxoids. In general, $\tilde{v}(q)$ is a rather complicated function of d_p, λ_p, d_s, λ_s, d_i, and the magnitude of q. It is real and negative, and its magnitude is a monotonically decreasing function of q. In the limit as $q \to 0$, the exact expression for $\tilde{v}(q)$ reduces to

$$\tilde{v}(q) \approx -(\varphi_0^2/4\pi q^2)[\lambda_p \coth(d_p/\lambda_p) + \lambda_s \coth(d_s/\lambda_s) + d_i]^{-1} \ , \tag{2.5}$$

and, when $q \gg \lambda_p^{-1}$ and λ_s^{-1}, which we shall call the large-q approximation, we have

$$\tilde{v}(q) \approx -(\varphi_0^2/8\pi\lambda_p^2\lambda_s^2 q^5) e^{-qd_i} \times (1 - e^{-qd_p})(1 - e^{-qd_s}) \ . \tag{2.6}$$

Once $\tilde{v}(q)$ is obtained, the coupling force $\vec{F}_c(\vec{s})$ exerted upon a secondary fluxoid for primary-lattice displacement $\vec{s}$ may be expressed as the gradient of $E_c(\vec{s})$. From Eq. (2.4) we obtain

$$\vec{F}_c(\vec{s}) = \nabla_s E_c(\vec{s}) = iA^{-1} \sum_{\vec{g}}{}' \vec{g} \tilde{v}(g)\, e^{i\vec{g}\cdot\vec{s}} \ . \tag{2.7}$$

For numerical computations it is convenient to choose as direct- and reciprocal-lattice vectors $\vec{l}_{mn} = m\vec{a}_1 + n\vec{a}_2$ and $\vec{g}_{mn} = 2\pi(m\vec{b}_1 + n\vec{b}_2)$, where m and n are integers and the fundamental lattice vectors are

$$\vec{a}_1 = d\hat{x}, \quad \vec{a}_2 = \tfrac{1}{2}d(\hat{x} + \hat{y}\sqrt{3}) \ ; \qquad \vec{b}_1 = d^{-1}(\hat{x} - \hat{y}/\sqrt{3}) \ , \quad \vec{b}_2 = (2/d\sqrt{3})\hat{y} \ . \tag{2.8}$$

The length of a reciprocal-lattice vector is $g_{mn} = (4\pi/d\sqrt{3})(m^2 - mn + n^2)^{1/2}$. It is sometimes also useful to introduce coordinates X and Y via

$$\vec{s} = X\vec{a}_1 + Y\vec{a}_2 \ , \tag{2.9}$$

such that

$$\vec{g}_{mn} \cdot \vec{s} = 2\pi(mX + nY) \ . \tag{2.10}$$

The coupling energy and coupling force then may be written as

$$E_c(X, Y) = \sum_{mn}{}' u_{mn}(1 - e^{i2\pi(mX+nY)}) \ , \tag{2.11}$$

$$\vec{F}_c(X, Y) = -i\left(\frac{4\pi}{3d^2}\right) \sum_{mn}{}' [(2m - n)\vec{a}_1 + (2n - m)\vec{a}_2] u_{mn} e^{i2\pi(mX+nY)} \ , \tag{2.12}$$

where

$$u_{mn} = -A^{-1}\tilde{v}(g_{mn}) \tag{2.13}$$

and the sum includes all integer values of m and n except the term for which $m = n = 0$.

For small s ($s \ll d$), $E_c(\vec{s})$ is quadratic in s,

$$E_c(\vec{s}) \approx \tfrac{1}{2}ks^2, \quad s \ll d \tag{2.14}$$

forming an isotropic potential well for the secondary fluxoid, such that the coupling force $\vec{F}_c(\vec{s})$ is isotropic and linear in $\vec{s}$. That is,

$$\vec{F}_c(\vec{s}) = k\vec{s}, \quad s \ll d \tag{2.15}$$

where

$$k = \frac{1}{2} \sum_{mn}{}' g_{mn}^2 u_{mn} \ . \tag{2.16}$$

These results may be derived by expanding the exponentials in Eqs. (2.11) and (2.12) and using the relations

$$2\sum_{mn}{}' mn\, u_{mn} = \sum_{mn}{}' m^2 u_{mn} = \sum_{mn}{}' n^2 u_{mn} \ , \tag{2.17}$$

which follow from the symmetry of $\vec{g}_{mn}$.

At sufficiently low fluxoid density, the summation over reciprocal-lattice vectors in Eq. (2.4) may be expressed as an integral over q. When $s \ll d$, we then may replace the argument $\vec{g}$ by $\vec{q}$ and $\sum_{\vec{g}}'$ by $A(2\pi)^{-2}\int d^2q$, where $A(2\pi)^{-2}$ is the density of reciprocal-lattice sites, to obtain

$$E_c(\vec{s}) \approx (2\pi)^{-2} \int d^2q\, \tilde{v}(q)(e^{i\vec{q}\cdot\vec{s}} - 1) = v(0, \vec{s}) \ . \tag{2.18}$$

Referring to Eq. (2.1), we see that Eq. (2.18) simply states that at sufficiently low flux density the dominant contribution to the coupling energy arises from the interaction between the secondary fluxoid and the nearest primary fluxoid.

At very low fluxoid density the coupling force is

thus optimized and is given by

$$\vec{F}_c(\vec{s}) \approx \nabla_s v(0, \vec{s}) . \tag{2.19}$$

Recently, Sherrill[7] calculated this force in the approximation $d_p \ll \lambda_p$ and $d_s \ll \lambda_s$. His result yields the correct order of magnitude for the full coupling force in thin films at sufficiently low flux density that the intervortex spacing d is large by comparison with the superconducting film thicknesses d_p and d_s.

At sufficiently high fluxoid density, the summation of Eq. (2.4) involves values of $\vec{g}$ for which the magnitude of $\tilde{v}(g)$ is decreasing rapidly with increasing g. It is then a good approximation to retain only those terms in the summation involving the six shortest reciprocal-lattice vectors of length $g_{10} = 4\pi/d\sqrt{3}$. We call this the one-reciprocal-lattice-vector approximation. From Eq. (2.11) we thus find

$$E_c(X, Y) \approx 2u_{10}[3 - \cos 2\pi X - \cos 2\pi Y - \cos 2\pi(X+Y)] . \tag{2.20}$$

Contours of constant E_c within the unit cell are shown in Fig. 1.

The minimum values of E_c ($E_c = 0$) occur when the primary fluxoids are located directly under the secondary fluxoids at the points F (integer X and Y). The maximum values of E_c ($E_c = E_{c\,\max} = 9u_{10}$) occur when the primary fluxoids are directly underneath the points C ($X = Y = \frac{1}{3}$ and $X = Y = \frac{2}{3}$), the centers of the equilateral triangles formed by the secondary fluxoids. Saddle points S, at which $E_c = \frac{1}{9}(8E_{c\,\max}) = 8u_{10}$, occur when the primary fluxoids are directly underneath the midpoints of lines connecting adjacent fluxoids in the secondary lattice, where $(X, Y) = (\frac{1}{2}, 0)$, $(0, \frac{1}{2})$, $(\frac{1}{2}, \frac{1}{2})$, $(1, \frac{1}{2})$, or $(\frac{1}{2}, 1)$.

The corresponding force $\vec{F}_c$ is normal to the contours shown in Fig. 1, and its magnitude is inversely proportional to the distance between adjacent contours. The maximum force is very nearly isotropic. In the one-reciprocal-lattice-vector approximation, Eq. (2.12) yields

$$\vec{F}_c(X, Y) = (8\pi/3d^2)u_{10}\{\vec{a}_1[2\sin 2\pi X + \sin 2\pi(X+Y) - \sin 2\pi Y] + \vec{a}_2[2\sin 2\pi Y + \sin 2\pi(X+Y) - \sin 2\pi X]\} . \tag{2.21}$$

For displacements $\vec{s}$ along the line FSF of Fig. 1 we obtain

$$\vec{F}_c = F_{cx}\hat{x} = (8\pi u_{10}/d)\sin(2\pi s/d)\hat{x} , \tag{2.22}$$

which has maximum magnitude $F_{cx\,\max} = 8\pi u_{10}/d$ at $s = 0.250d$. For $\vec{s}$ along the line $FCSCF$, we obtain

$$\vec{F}_c = F_{cs}\hat{u} = (16\pi u_{10}/d_1)\sin(3\pi s/d_1) \times \cos(\pi s/d_1)\hat{u} , \tag{2.23}$$

where $d_1 = d\sqrt{3}$ and $\hat{u} = \vec{s}/s$. The maximum magnitude of F_{cs}, $F_{cs\,\max} = 1.016\, F_{cx\,\max}$, occurs at $s = 0.258d$. Both F_{cx} and F_{cs} are plotted in Fig. 2.

We may use the one-reciprocal-lattice-vector approximation at this point to obtain the qualitative behavior of $F_{cx\,\max}$ as a function of flux density B. Combining the above result with Eqs. (2.13) and (2.6), we obtain

$$F_{cx\,\max} \approx (3\varphi_0^2/32\pi^3\lambda_p^2\lambda_s^2 g_{10}^2)e^{-\varepsilon_{10}d_i} \times (1 - e^{-\varepsilon_{10}d_p})(1 - e^{-\varepsilon_{10}d_s}) . \tag{2.24}$$

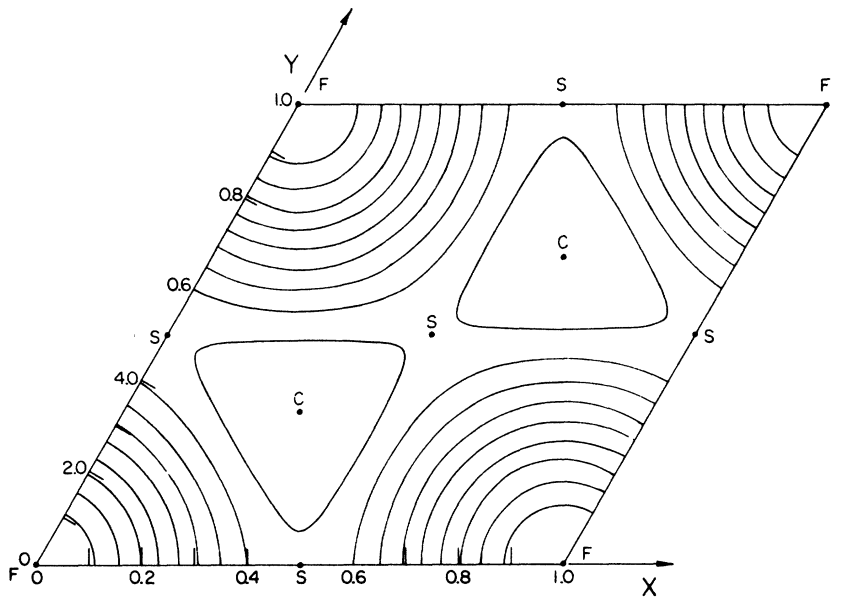

FIG. 1. Contours of the coupling energy $E_c(\vec{s})$ as a function of the primary lattice displacement $\vec{s}$, for $\vec{s}$ within the unit cell of the triangular lattice. Contours are calculated from Eq. (2.20) for $E_c/E_{c\,\max} = 0.1$, 0.2, ..., 0.9. Minima ($E_c = 0$) occur under the secondary fluxoids at points F. Maxima ($E_{c\,\max} = 9u_{10}$) occur at points C. Saddle points ($E_c = 8u_{10}$) occur at points S.

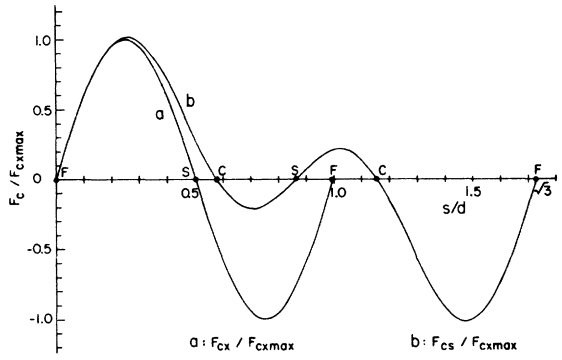

FIG. 2. Coupling force exerted on a secondary fluxoid for primary-lattice displacements along symmetry directions of Fig. 1. Shown are (a) along FSF, $F_{cx}/F_{cx\max} = \sin(2\pi s/d)$ [Eq. (2.22)] and (b) along $FCSCF$, $F_{cs}/F_{cx\max}$ [Eq. (2.23)], where $F_{cx\max} = 8\pi u_{10}/d$ and d is the nearest-neighbor distance. The maximum coupling force is nearly the same for the two directions.

We see that, since $B = g_{10}^2(\varphi_0\sqrt{3}/8\pi^2)$, Eq. (2.24) yields $F_{cx\max} \propto B^{-1}$ in the field range for which g_{10} obeys λ_p^{-1}, λ_s^{-1}, d_p^{-1}, $d_s^{-1} \ll g_{10} \ll d_i^{-1}$ or, alternatively, for which the intervortex spacing d obeys $d_i \ll d \ll d_p$, d_s, λ_p, λ_s.

In general, we may say that at low flux density the maximum coupling force saturates at a value of the order of the maximum primary-secondary-fluxoid-pair–interaction force. With increasing flux density the effect of the field contributions of adjacent fluxoids is to smooth out the inhomogeneities in the magnetic field between the films, to decrease the amplitude of the oscillation in E_c versus $\vec{s}$, and thereby to reduce the magnitude of the maximum coupling force, roughly as B^{-1}. Eventually, when the interfluxoid spacing d is of the order of the insulator thickness d_i or smaller, the field presented at the secondary by the primary lattice is extremely homogeneous, and, as is seen from Eq. (2.24), the maximum coupling force decreases exponentially with further increase of B.

III. EQUATIONS OF MOTION

A. Derivation of equations

For simplicity, we consider only the case for which the primary- and secondary-fluxoid motion is in the $\pm x$ direction, parallel to a lattice vector. In the following we thus assume that $\vec{s} = s_x\hat{x}$ and that $\vec{F}_c(\vec{s}) = F_{cx}(s_x)\hat{x}$, where $F_{cx}(s+d) = F_{cx}(s)$. For further simplicity, we shall use in the following calculations the coupling-force model $F_{cx}(s_x) = F_m \times \sin(2\pi s_x/d)$, where F_m is to be regarded as a function of d and the specimen parameters λ_p, λ_s, d_p, d_s, and d_i. A sinusoidal model was first used by Cladis, Parks, and Daniels[2] and is justified in the one-reciprocal-lattice-vector approximation, as is seen from Eq. (2.22).

We write now the equations of motion for the primary and secondary fluxoids. We allow for the possibility of a transport current density J_{py} (J_{sy}) in the y direction in the primary (secondary), which exerts a Lorentz force per unit length $J_{py}\varphi_0/c$ ($J_{sy}\varphi_0/c$) upon the primary (secondary) fluxoids.[8] We may represent the combined strength of surface and bulk pinning in the primary (secondary) films by the critical current density J_{pc} (J_{sc}). The driving force in the x direction on a fluxoid is $J_{py}\varphi_0 d_p/c - F_{cx}(s_x)$ in the primary and $J_{sy}\varphi_0 d_s/c + F_{cx}(s_x)$ in the secondary. When the magnitude of the driving force is less than $J_{pc}\varphi_0 d_p/c$ ($J_{sc}\varphi_0 d_s/c$) there will be no fluxoid motion in the primary (secondary). However, when the magnitude of the driving force exceeds this value, flux motion results. Assuming negligibly small Hall angle, the net force on a fluxoid in such a case is balanced by a viscous-drag force $\eta_p \dot{x}_p d_p$ ($\eta_s \dot{x}_s d_s$), where η_p (η_s) is a field-dependent viscous-drag coefficient and $\dot{x}_p$ ($\dot{x}_s$) is the x component of the fluxoid speed in the primary (secondary). The y component of the electric field generated by this motion is

$$E_{py} = \dot{x}_p B/c = \rho_p[J_{py} \mp J_{pc} - cF_{cx}(s_x)/\varphi_0 d_p] \tag{3.1}$$

in the primary, and

$$E_{sy} = \dot{x}_s B/c = \rho_s[J_{sy} \mp J_{sc} + cF_{cx}(s_x)/\varphi_0 d_s] \tag{3.2}$$

in the secondary, where $\rho_p = \varphi_0 B/\eta_p c^2$ ($\rho_s = \varphi_0 B/\eta_s c^2$) is the primary (secondary) flux-flow resistivity and B is the magnetic flux density in the films. The upper (lower) sign holds when the y component of the electric field is positive (negative).

It is convenient to introduce $V_p = L_y \dot{x}_p B/c$ ($V_s = L_y \dot{x}_s B/c$), the voltage measured across length L_y, and I_p (I_s), the current through width L_x and thickness d_p (d_s) of the primary (secondary) film. Equations (3.1) and (3.2) may then be written compactly as

$$V_p = (\delta I_p^{\pm} - I_{ps})R_p , \tag{3.3}$$

$$V_s = (\delta I_s^{\pm} + I_{ps})R_s , \tag{3.4}$$

where

$$\delta I_p^{\pm} = I_p \mp I_{pc} , \tag{3.5}$$

$$\delta I_s^{\pm} = I_s \mp I_{sc} , \tag{3.6}$$

$$I_p = J_{py} L_x d_p , \tag{3.7}$$

$$I_s = J_{sy} L_x d_s , \tag{3.8}$$

$$I_{pc} = J_{pc} L_x d_p , \tag{3.9}$$

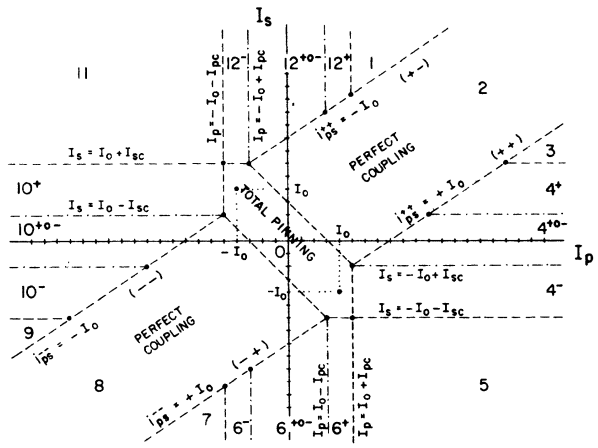

FIG. 3. $I_p - I_s$ map for magnetically coupled films with relatively weak pinning and parameters in the ratios $I_{pc}:I_{sc}:I_0 = 1:2:4$ and $R_p:R_s = 2:3$. The behavior of the current-voltage characteristics in each numbered region is discussed in the text and summarized in Table I.

$$I_{sc} = J_{sc} L_x d_s \,, \tag{3.10}$$

$$R_p = L_y \rho_p / L_x d_p \,, \tag{3.11}$$

$$R_s = L_y \rho_s / L_x d_s \,, \tag{3.12}$$

$$I_{ps} = cF_{cx}(s_x) L_x / \varphi_0 = I_0 \sin(2\pi s_x / d) \,, \tag{3.13}$$

$$I_0 = cF_m L_x / \varphi_0 \,. \tag{3.14}$$

The upper (lower) signs hold when the voltage is positive (negative). As we shall see shortly, the current-voltage characteristics of the time-averaged voltages $\overline{V}_p$ and $\overline{V}_s$ versus I_p and I_s depend upon only *five* parameters: I_{pc} (I_{sc}), the depinning critical current of the primary (secondary) alone; R_p (R_s), the flux-flow resistance of the primary (secondary) alone; and I_0, a quantity we call the coupling current, which is proportional to the maximum coupling force.

B. Results with weak pinning

To understand the current-voltage characteristics dictated by Eqs. (3.3) and (3.4) under conditions of relatively weak pinning, it is helpful to consider an I_p-I_s map, shown in Fig. 3, which is drawn for parameters in the ratios $I_{pc}:I_{sc}:I_0 = 1:2:4$ and $R_p:R_s = 2:3$. For combinations of I_p and I_s that fall within the six-sided region (labeled region 0) centered on the origin, bounded by the lines $I_p = I_0 + I_{pc}$, $I_p = -I_0 - I_{pc}$, $I_s = I_0 + I_{sc}$, $I_s = -I_0 - I_{sc}$, $I_p + I_s = I_{pc} + I_{sc}$, and $I_p + I_s = -I_{pc} - I_{sc}$, *total pinning* occurs; that is, there is no flux motion in either film, and $V_p = V_s = 0$. When $I_s = 0$, for example, as shown in Fig. 4, total pinning ($V_p = V_s = 0$) occurs for I_p in the range $|I_p| < I_{pc} + I_{sc}$.

For combinations of I_p and I_s that fall within regions 2 or 8 on the I_p-I_s map, *perfect coupling* occurs. Here the combined Lorentz force from currents in the two films is sufficient to depin both the primary and secondary fluxoids; that is, $|I_p + I_s| > I_{pc} + I_{sc}$. Furthermore, the coupling between the primary and secondary fluxoids is sufficiently strong that the two lattices are locked together with a fixed relative displacement $|s_x| < \frac{1}{4}d$, and they move at constant speed parallel to the x axis. Eliminating I_{ps} from Eqs. (3.3) and (3.4), we find that the common voltage in the two films under conditions of perfect coupling is

$$V_\pm = (\delta I_p^\pm + \delta I_s^\pm) R \,, \tag{3.15}$$

where the upper (lower) sign holds for positive (negative) voltage and

$$R^{-1} = R_p^{-1} + R_s^{-1} \,. \tag{3.16}$$

When $I_s = 0$, for example, as shown in Fig. 4, perfect coupling ($V_p = V_s = V_+$) occurs along the line AB, given by $V_+ = (I_p - I_{pc} - I_{sc})R$.

Inserting Eq. (3.15) into Eq. (3.3) and solving for I_{ps}, we obtain

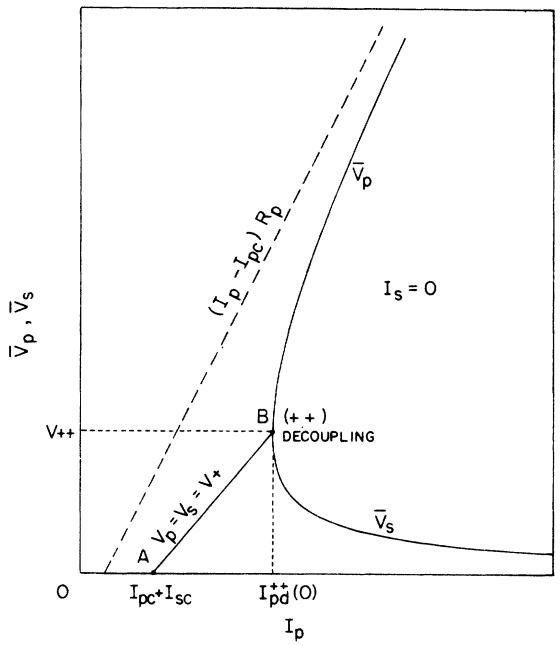

FIG. 4. Time-averaged primary and secondary voltages $\overline{V}_p$ and $\overline{V}_s$ vs primary current I_p when $I_s = 0$ for weakly pinned, magnetically coupled films with parameters in the ratios $I_{pc}:I_{sc}:I_0 = 1:2:4$ and $R_p:R_s = 2:3$. For $0 < I_p < I_{pc} + I_{sc}$, total pinning (region 0 of Fig. 3) occurs, and $V_p = V_s = 0$. Along line AB, which has slope R ($R^{-1} = R_p^{-1} + R_s^{-1}$), perfect coupling (region 2) occurs, and $V_p = V_s = V_+$. At point B, where $V_p = V_s = V_{++} = (I_0 - I_{sc})R_s$ and $I_p = I_{pd}^{++}(0) = I_{pc} - I_{sc}R_s/R_p + I_0 R_t/R_p$, where $R_t = R_p + R_s$, the (++) decoupling condition occurs. For $I_p > I_{pd}^{++}(0)$, the films are partially decoupled (region 4^{+0-}). For large I_p, $\overline{V}_s$ approaches $(I_p - I_{pc})R_p$ (dashed).

$$\sin(2\pi s_x/d) = i_{ps}^{\pm\pm}/I_0 , \tag{3.17}$$

where

$$i_{ps}^{\pm\pm} = (\delta I_p^{\pm} R_p - \delta I_s^{\pm} R_s)/R_t , \tag{3.18}$$

$$R_t = R_p + R_s . \tag{3.19}$$

The first sign of $i_{ps}^{\pm\pm}$ is associated with $\delta I_p^{\pm}$ and the second with $\delta I_s^{\pm}$. In the perfect-coupling regions the magnitude of $\sin(2\pi s_x/d)$ in Eq. (3.17) does not exceed unity. When the magnitude of $i_{ps}^{\pm\pm}$ [Eq. (3.18)] exceeds I_0, however, partial decoupling of the primary- and secondary-fluxoid lattice occurs and one lattice begins to slip relative to the other. Four conditions at decoupling are possible; let us label these the (++), (+−), (−+), and (− −) decoupling conditions, where the first sign of a pair refers to the sign of V and the second refers to the sign of $i_{ps}^{\pm\pm}$ and $I_{ps} = I_0 \sin(2\pi s_x/d)$ at the onset of slippage. When $I_s = 0$, for example, as shown in Fig. 4, the (++) decoupling condition, where $i_{ps}^{\pm\pm} = +I_0$, is reached at point B. In general, the four decoupling conditions are reached along four corresponding lines on the I_p-I_s map given by the solutions of $|i_{ps}^{\pm\pm}| = I_0$. With the help of Eq. (3.18) we find that the slope of each decoupling line is

$$\frac{dI_s}{dI_p} = \frac{R_p}{R_s} . \tag{3.20}$$

As will become clear in Ref. 3, to assist in the experimental evaluation of the parameters I_{pc}, I_{sc}, R_p, R_s, and I_0, it is useful to denote by $V_{\pm\pm}$ the voltage $V_p = V_s$ at the (±±) decoupling condition. From Eqs. (3.3) and (3.4) we obtain

$$V_{\pm\pm} = (\delta I_p^{\pm} \mp I_0)R_p = (\delta I_s^{\pm} \pm I_0)R_s . \tag{3.21}$$

From this equation we find that the value of I_p at the (±±) decoupling condition as a function of I_s is

$$I_{pd}^{\pm\pm}(I_s) \equiv \pm I_{pc} + (I_s \mp I_{sc})R_s/R_p \pm I_0 R_t/R_p . \tag{3.22}$$

Similarly, the value of I_s at the (±±) decoupling condition as a function of I_p is

$$I_{sd}^{\pm\pm}(I_p) \equiv \pm I_{sc} + (I_p \mp I_{pc})R_p/R_s \mp I_0 R_t/R_p . \tag{3.23}$$

Finally, we denote the combination of values of I_p and I_s that makes $V_{\pm\pm}$ zero by

$$I_{p\pm\pm} = \pm I_{pc} \pm I_0 , \tag{3.24}$$

$$I_{s\pm\pm} = \pm I_{sc} \mp I_0 . \tag{3.25}$$

In Eqs. (3.21)–(3.25) the first upper (lower) sign in (±±) is associated with the upper (lower) signs preceding I_{pc} and I_{sc}, and the second upper (lower) sign in (±±) is associated with the sign preceding I_0.

When $I_s = 0$, for example, as shown in Fig. 4, the (++) decoupling condition at point B is characterized by

$$V_{++}(I_s = 0) = (I_0 - I_{sc})R_s , \tag{3.26}$$

$$I_{pd}^{++}(0) = I_{pc} - I_{sc}R_s/R_p + I_0 R_t/R_p . \tag{3.27}$$

Returning to the I_p-I_s map of Fig. 3 we note that there are six regions (1, 3, 5, 7, 9, and 11) for which the combinations of I_p and I_s are such that, although the primary and secondary lattices are slipping relative to each other, neither lattice ever comes instantaneously to rest. For these regions, whose boundaries are listed in Table I, the combination of the Lorentz force and the coupling force in each film is always sufficient to exceed the pinning force, producing a nonzero, though time-varying, fluxoid speed. Subtracting Eq. (3.4) from Eq. (3.3) and making use of $\dot{x}_p - \dot{x}_s = \dot{s}_x$, we obtain a differential equation for s_x versus time,

$$V_{ps} = V_p - V_s = (L_y B/c)\dot{s}_x = [i_{ps}^{\pm\pm} - I_0 \sin(2\pi s_x/d)]R_t . \tag{3.28}$$

The slippage period τ, the time required for s_x to change by a distance d, is easily found by integration to be

$$\tau = (L_y B d/c R_t)[(i_{ps}^{\pm\pm})^2 - I_0^2]^{-1/2} , \tag{3.29}$$

such that the time average of Eq. (3.28) is

$$\overline{V}_{ps} = \overline{V}_p - \overline{V}_s = (i_{ps}^{\pm\pm} - \overline{I}_{ps})R_t = i_{ps}^{\pm\pm} R_t [1 - I_0^2/(i_{ps}^{\pm\pm})^2]^{1/2} . \tag{3.30}$$

Thus, in regions 1, 3, 5, 7, 9, and 11, the time-averaged primary and secondary voltages are given by

$$\overline{V}_p = (\delta I_p^{\pm} - \overline{I}_{ps})R_p , \tag{3.31}$$

$$\overline{V}_s = (\delta I_s^{\pm} + \overline{I}_{ps})R_s , \tag{3.32}$$

where

$$\overline{I}_{ps} = i_{ps}^{\pm\pm}\{1 - [1 - I_0^2/(i_{ps}^{\pm\pm})^2]^{1/2}\} , \tag{3.33}$$

a result similar to that of Cladis, Parks, and Daniels.[2]

Returning to the I_p-I_s map of Fig. 3, there are four remaining regions, 4, 6, 10, and 12, for which the fluxoid motion in the primary and secondary films is considerably more complicated than that described above. In regions 4^{+0-}, 6^{+0-}, 10^{+0-}, and 12^{+0-}, for example, while one of the lattices is continuously advancing, the other lattice may first move forward, be pinned, move backward, be pinned, then move forward, all during one cycle, provided the coupling between the films is sufficiently large. The behavior in regions 4, 6, 10, and 12 is summarized in Table I.

To compute the primary and secondary voltages in regions 4, 6, 10, and 12, therefore, we derive from Eqs. (3.3) and (3.4) differential equations for

TABLE I. Summary of the behavior of the primary and secondary voltages V_p and V_s in the regions of the $I_p - I_s$ plane bounded by dashed lines shown in Figs. 3 and 8.

Region	Definition[a]	V_p	V_s	$\overline{V}_p$ and $\overline{V}_s$	Comments
0	$\lvert I_p - I_{ps}\rvert < I_{pc}$ $\lvert I_s + I_{ps}\rvert < I_{sc}$	0	0	$\overline{V}_p = \overline{V}_s = 0$	Total primary and secondary pinning
1	$\delta I_p^+ > I_0$ $i_{ps}^{+-} < -I_0$	+	+	$0 < \overline{V}_p < \overline{V}_s$	Partial decoupling
2	$\delta I_p^+ + \delta I_s^+ > 0$ $\lvert i_{ps}^{+-}\rvert < I_0$	+	+	$\overline{V}_p = \overline{V}_s = V_+$	Perfect coupling
3	$\delta I_s^+ > I_0$ $i_{ps}^{+-} > I_0$	+	+	$0 < \overline{V}_s < \overline{V}_p$	Partial decoupling
4	$\delta I_p^+ > I_0$ $\lvert I_s\rvert < I_0 + I_{sc}$ $i_{ps}^{+-} > I_0$	+	+, 0, −	$\overline{V}_s < \overline{V}_p$	Partial decoupling
4^+	$I_s > \lvert I_{sc} - I_0\rvert$	+	+, 0	$0 < \overline{V}_s < \overline{V}_p$	Partial secondary pinning
4^0	$I_{sc} > I_0$: $\lvert I_s\rvert < I_{sc} - I_0$	+	0	$\overline{V}_s = 0 < \overline{V}_p$	Total secondary pinning
or					
4^{+0-}	$I_0 > I_{sc}$: $\lvert I_s\rvert < I_0 - I_{sc}$	+	+, 0, −	$\overline{V}_s < \overline{V}_p$	Partial secondary pinning
4^-	$I_s < -\lvert I_{sc} - I_0\rvert$	+	0, −	$\overline{V}_s < 0 < \overline{V}_p$	Partial secondary pinning
5	$\delta I_p^+ > I_0$ $\delta I_s^- < -I_0$ $i_{ps}^{+-} > I_0$	+	−	$\overline{V}_s < 0 < \overline{V}_p$	Partial decoupling
6	$\delta I_s^- < -I_0$ $\lvert I_p\rvert < I_0 + I_{pc}$ $i_{ps}^{--} > I_0$	+, 0, −	−	$\overline{V}_s < \overline{V}_p$	Partial decoupling
6^+	$I_p > \lvert I_{pc} - I_0\rvert$	+, 0	−	$\overline{V}_s < 0 < \overline{V}_p$	Partial primary pinning
6^0	$I_{pc} > I_0$: $\lvert I_p\rvert < I_{pc} - I_0$	0	−	$\overline{V}_s < \overline{V}_p = 0$	Total primary pinning
or					
6^{+0-}	$I_0 > I_{pc}$: $\lvert I_p\rvert < I_0 - I_{pc}$	+, 0, −	−	$\overline{V}_s < \overline{V}_p$	Partial primary pinning
6^-	$I_p < -\lvert I_{pc} - I_0\rvert$	0, −	−	$\overline{V}_s < \overline{V}_p < 0$	Partial primary pinning

TABLE I. (*Continued*)

Region	Definition[a]	V_p	V_s	$\bar{V}_p$ and $\bar{V}_s$	Comments
7	$\delta I_p^- < -I_0$ $i_{ps}^{--} > I_0$	−	−	$\bar{V}_s < \bar{V}_p < 0$	Partial decoupling
8	$\delta I_p^- + \delta I_s^- < 0$ $\lvert i_{ps}^{+-} \rvert < I_0$	−	−	$\bar{V}_s = \bar{V}_p = V_-$	Perfect coupling
9	$\delta I_s^- < -I_0$ $i_{ps}^{--} < -I_0$	−	−	$\bar{V}_p < \bar{V}_s < 0$	Partial decoupling
10	$\lvert I_s \rvert < I_0 + I_{sc}$ $\delta I_p^- < -I_0$ $i_{ps}^{--} < -I_0$	−	+, 0, −	$\bar{V}_p < \bar{V}_s$	Partial decoupling
10^-	$I_s < -\lvert I_{sc} - I_0 \rvert$	−	0, −	$\bar{V}_p < \bar{V}_s < 0$	Partial secondary pinning
10^0	$I_{sc} > I_0$: $\lvert I_s \rvert < I_{sc} - I_0$	−	0	$\bar{V}_p < \bar{V}_s = 0$	Total secondary pinning
or					
10^{+0-}	$I_0 > I_{sc}$: $\lvert I_s \rvert < I_0 - I_{sc}$	−	+, 0, −	$\bar{V}_p < \bar{V}_s$	Partial secondary pinning
10^+	$I_s > \lvert I_{sc} - I_0 \rvert$	−	+, 0	$\bar{V}_p < 0 < \bar{V}_s$	Partial secondary pinning
11	$\delta I_s^+ > I_0$ $\delta I_p^- < -I_0$ $i_{ps}^{+-} < -I_0$	−	+	$\bar{V}_p < 0 < \bar{V}_s$	Partial decoupling
12	$\lvert I_p \rvert < I_0 + I_{pc}$ $\delta I_s^+ > I_0$ $i_{ps}^{++} < -I_0$	+, 0, −	+	$\bar{V}_p < V_s$	Partial decoupling
12^-	$I_p < -\lvert I_{pc} - I_0 \rvert$	0, −	+	$\bar{V}_p < 0 < \bar{V}_s$	Partial primary pinning
12^0	$I_{pc} > I_0$: $\lvert I_p \rvert < I_{pc} - I_0$	0	+	$\bar{V}_p = 0 < \bar{V}_s$	Total primary pinning
or					
12^{+0-}	$I_0 > I_{pc}$: $\lvert I_p \rvert < I_0 - I_{pc}$	+, 0, −	+	$\bar{V}_p < \bar{V}_s$	Partial primary pinning
12^+	$I_p > \lvert I_{pc} - I_0 \rvert$	+, 0	+	$0 < \bar{V}_p < \bar{V}_s$	Partial primary pinning

[a] $\delta I_p^{\pm} = I_p \mp I_{pc}$, $\delta I_s^{\pm} = I_s \mp I_{sc}$, and $i_{ps}^{\pm\pm} = (\delta I_p^{\pm} R_p - \delta I_s^{\pm} R_s)/(R_p + R_s)$.

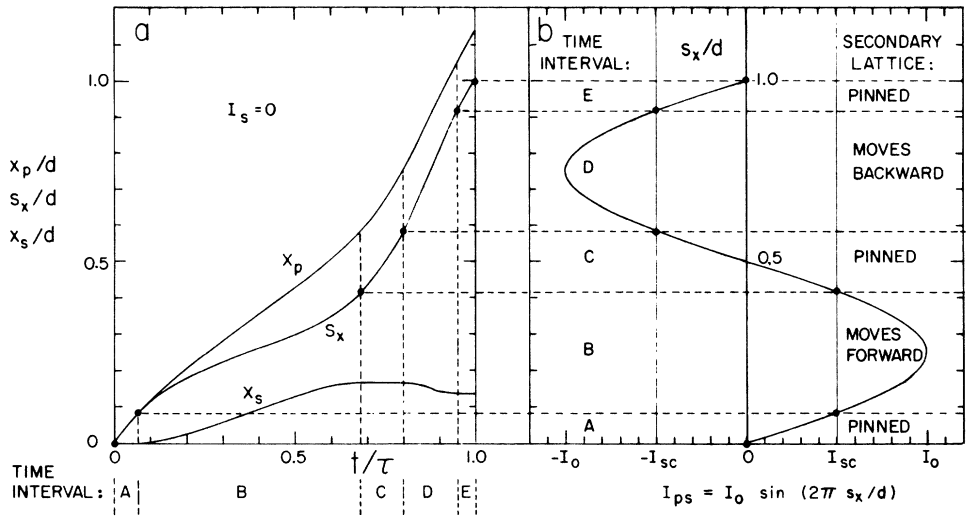

FIG. 5. (a) Reduced displacements x_p/d, $s_x/d = (x_p - x_s)/d$, and x_s/d vs reduced time t/τ under conditions of partial decoupling for $I_s = 0$ and ratios $I_{pc} : I_{sc} : I_0 : I_p = 1 : 1 : 2 : 5$ and $R_p : R_s = 1 : 1$. Note that $\bar{s}_x = d/\tau$, where d is the nearest-neighbor distance. The slippage period τ, calculated from Eqs. (3.3) and (3.4) of the text, is here $\tau = 0.361 L_y B d/c I_{pc} R_p$, such that $\bar{V}_{ps} = \bar{V}_p - \bar{V}_s = L_y B d/c\tau = 2.77 I_{ps} R_p$. Similarly, $\bar{V}_p = L_y B \bar{s}_x/c = 3.14 I_{pc} R_p$ and $\bar{V}_s = L_y B \bar{x}_s/c = 0.37 I_{pc} R_p$. (b) Coupling current $I_{ps} = I_0 \sin(2\pi s_x/d)$ vs reduced primary-secondary displacement s_x/d. As seen from Eq. (3.4) of the text, when $I_s = 0$ the value of I_{ps} relative to $\pm I_{sc}$ determines the time intervals during which the secondary lattice is pinned (A, C, E), moves forward (B), or moves backward (D).

s_x versus time t similar to Eq. (3.28). However, two or three such equations are necessary to describe a complete cycle, during which, at various times, one of the lattices moves forward, is pinned, or even moves backward.

Figure 5 illustrates the resulting behavior of $x_s(t)$, $x_p(t)$, and $s_x(t) = x_p - x_s$ versus time t for a typical point on the I_p axis in region 4. Since here $I_s = 0$, the motion of the secondary fluxoids is governed by the ratio of the coupling force to the pinning force. In time intervals A, C, and E, when the pinning force exceeds the magnitude of the coupling force ($I_0 < |I_{sc}|$), the secondary fluxoids are pinned; in time interval B, when the coupling force exceeds the pinning force ($I_{ps} > I_{sc}$), the secondary fluxoids are driven in the forward direction; in time interval D, when the magnitude of the negatively directed coupling force exceeds the pinning force ($I_{ps} < -I_{sc}$), the secondary fluxoids are driven backward. Although the maximum secondary-fluxoid speed is the same whether it moves backward or forward, the secondary fluxoids spend more time traveling forward than backward, thereby making net forward progress. The time-averaged voltages are $\bar{V}_p = L_y B x_p(\tau)/c\tau$, $\bar{V}_s = L_y B x_s(\tau)/c\tau$, and $\bar{V}_{ps} = \bar{V}_p - \bar{V}_s = L_y B d/c\tau$, where τ is the total time required for slippage by one lattice vector d.

When $I_s = 0$, it follows from the equations of motion that for larger values of I_p and faster motion of the primary fluxoids, the secondary fluxoids are increasingly unable to follow the primary lattice. As a result, the secondary fluxoids spend nearly as much time moving backward as moving forward, thereby making less net forward progress. Accordingly, the time-averaged secondary voltage $\bar{V}_s$ decreases monotonically with increasing I_p.

The qualitative behavior of V_p and V_s in the thirteen major regions of the I_p-I_s map of Fig. 3 is summarized in Table I. It is a straightforward problem to develop a computer program which computes $\bar{V}_p$ and $\bar{V}_s$ versus I_p and I_s for magnetically coupled films characterized by the five parameters I_{pc}, I_{sc}, R_p, R_s, and I_0. Shown in Fig. 6 is a computer-generated plot of $\bar{V}_s$ versus I_p for a series of values of I_s. The ratios of $I_{pc} : I_{sc} : I_0$ and $R_p : R_s$ are the same as those assumed for Fig. 3. Also identified in Fig. 6 are the portions of the $\bar{V}_s$-vs-I_p curves for which the behavior is characterized by the corresponding numbered regions in the I_p-I_s map of Fig. 3. Shown in Fig. 7 is the computer-generated plot of $\bar{V}_p$ versus I_p for the same parameters and values of I_s used for Fig. 6. Structure in this plot may be correlated with corresponding structure in Fig. 6.

C. Results with strong pinning

To obtain the results described above and displayed in Figs. 3–7, we have assumed implicitly that I_0 is sufficiently large that perfect coupling can occur when $I_s = 0$. When $0 < I_0 < I_{sc}$, however, since the maximum coupling force exerted by the primary lattice on a secondary fluxoid does not exceed the

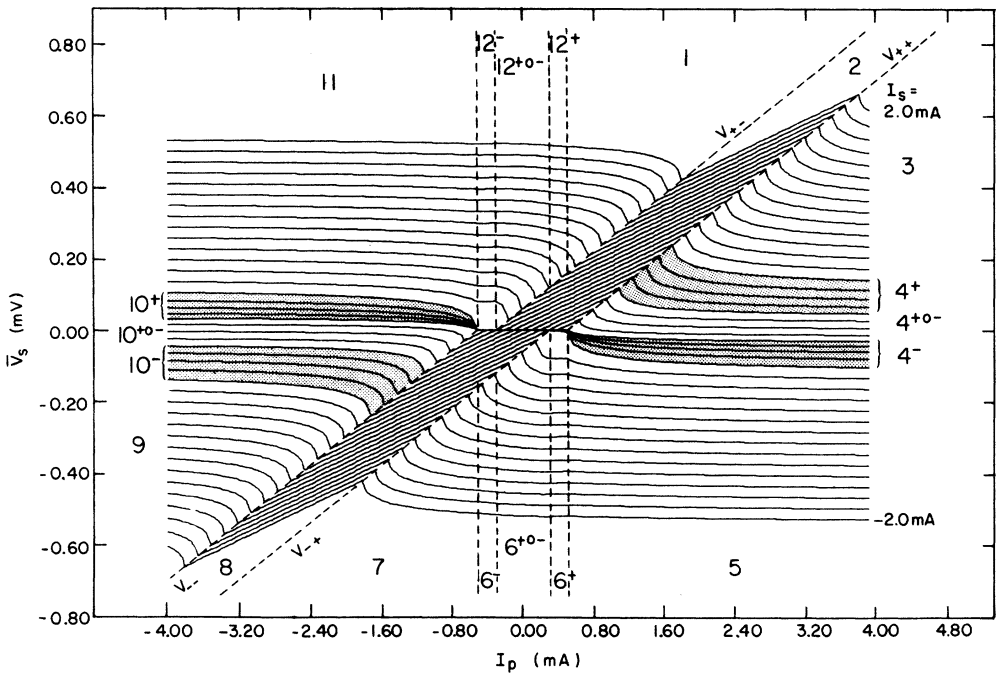

FIG. 6. Theoretical time-averaged secondary voltage $\bar{V}_s$ vs primary current I_p, calculated as described in the text for secondary currents $I_s = -2.0, -1.9, \ldots, 1.9, 2.0$ mA. Model parameters $I_{pc} = 0.1$ mA, $I_{sc} = 0.2$ mA, $I_0 = 0.4$ mA, $R_p = 0.2\ \Omega$, and $R_s = 0.3\ \Omega$ were selected to describe weakly pinned magnetically coupled films. Numbered regions correspond to those of the $I_p - I_s$ map of Fig. 3.

pinning force on it, we find that $\bar{V}_s = 0$ for $I_s = 0$, regardless of the value of I_p. The only manifestation of the presence of magnetic coupling in this case is the altered shape of $\bar{V}_p$ versus I_p. When $0 < I_p < I_{pc} + I_0$, we find $V_p = 0$, but when $I_p > I_p + I_0$, we find

$$\bar{V}_p = [(I_p - I_{pc})^2 - I_0^2]^{1/2} R_p \,, \tag{3.34}$$

which is obtained by solving Eqs. (3.3) and (3.13).

We may see more clearly the behavior of coupled films subject to relatively strong pinning by consulting Fig. 8, which is an I_p-I_s map appropriate to a hypothetical strongly pinned specimen with parameters in the ratios $I_{pc} : I_{sc} : I_0 = 3 : 4 : 1$ and $R_p : R_s = 2 : 3$. At the center of this map is the six-sided region 0, within which there is total pinning of both the primary and secondary lattices.

Within region 4^0, bounded by the lines $I_p = I_{pc} + I_0$, $I_s = I_{sc} - I_0$, and $I_s = -(I_{sc} - I_0)$, the secondary lattice remains totally pinned, but the primary lattice always moves forward under the combined influence of the Lorentz force, the pinning force, and the coupling force, yielding $\bar{V}_p$ versus I_0 as given by Eq. (3.34).

When a transport current is passed through the secondary lattice, the resulting Lorentz force may be sufficient, when acting in combination with the coupling force, to exceed the pinning force and to drive the secondary lattice into motion. In fact, when $I_p + I_s > I_{pc} + I_{sc}$ and $|i_{ps}^{\pm\pm}| < I_0$, which defines region 2 of Figs. 3 and 8, perfect coupling ($V_p = V_s = V_*$) may occur, just as discussed in Sec. III B.

The behavior under other combinations of I_p and I_s in Fig. 8 may be analyzed using the approach of Sec. III B and is summarized in Table I. Numerical computations of $\bar{V}_p$ and $\bar{V}_s$ versus I_p and I_s may be performed using the same computer program as discussed in Sec. III B. Shown in Fig. 9 is a computer-generated plot of $\bar{V}_s$ versus I_p for a series of values of I_s for a specimen whose ratios of $I_{pc} : I_{sc} : I_0$ and $R_p : R_s$ are the same as those assumed for Fig. 8. Also identified in Fig. 9 are the portions of the $\bar{V}_s$-vs-I_p curves for which the behavior is characterized by the corresponding numbered regions in Fig. 8. Shown in Fig. 10 is the associated plot of $\bar{V}_p$ versus I_p.

We note here that if there is any magnetic coupling at all between two films (that is, if $I_0 > 0$), then *a region of perfect coupling can always be achieved* for an appropriately chosen range of primary and secondary currents. As we have seen, this is true even for strongly pinned specimens for which, in the absence of a secondary current, primary-fluxoid motion produces no secondary-flux motion. This result yields a rule of thumb which may be useful experimentally: To determine the presence of magnetic coupling, one should look for structure in a plot of the secondary voltage versus

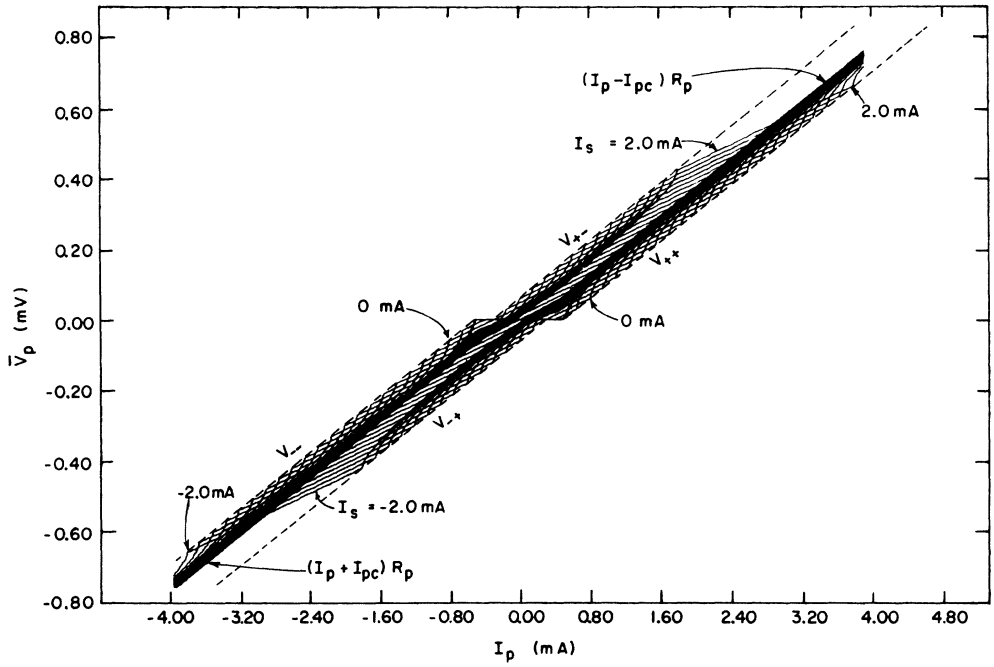

FIG. 7. Theoretical time-averaged primary voltage $\bar{V}_p$ vs primary current I_p for secondary currents $I_s = -2.0, -1.9, \ldots, 1.9, 2.0$ mA. Model parameters are those used for Fig. 6. The four dashed lines illustrate the decoupling voltages $V_{\pm\pm} = (I_p \mp I_{pc} \mp I_0)R_p$ [Eq. (3.21) of the text]. Note also that, for primary currents well above the decoupling current, $\bar{V}_p$ asymptotically approaches $(I_p - I_{pc})R_p$, regardless of the value of I_s.

the primary current—not just at zero secondary current, but also at secondary currents large enough to drive the secondary fluxoids into motion.

D. Results with weak pinning and passive secondary load

We return to the case of weak pinning considered in Sec. III B, for which $I_0 > I_{sc}$. We further consider the case for which any transport current in the secondary must return through a load resistance. One way to visualize the connection of the load resistance is to regard a portion of the secondary of length L_y, width L_x, and thickness d_s as being connected in series with load resistance R_L. The current carried in the y direction by the secondary, which must be returned in the opposite direction through the load, is $I_s = J_{sy} L_x d_s$. Since the voltage drop $V_s = E_{sy} L_y$ along L_y in the secondary must be equal to the voltage drop across the load resistance, we obtain

$$V_s = -I_s R_L . \tag{3.35}$$

Thus, in the presence of a load resistance, a secondary voltage induces a secondary current that, in turn, produces a Lorentz force in *opposition to the flux motion* producing the voltage. This result may be regarded simply as a consequence of Lenz's law.

Under conditions of perfect coupling, we may combine Eqs. (3.15) and (3.35) to obtain

$$V_\pm = [I_p \mp (I_{pc} + I_{sc})]R_{eff} , \tag{3.36}$$

where the upper (lower) sign holds for positive (negative) voltage, and

$$R_{eff}^{-1} = R_p^{-1} + R_s^{-1} + R_L^{-1} . \tag{3.37}$$

Under open-circuit conditions, when R_L is infinite, we obtain $I_s = 0$ and $R_{eff} = R$. The slope R_{eff} of $V_\pm$ versus I_p decreases monotonically with decreasing load resistance and vanishes under short-circuit conditions when R_L vanishes. Equations (3.36) and (3.37) thus justify the corresponding empirical formulas derived by Giaever on the basis of his experiments.[1]

The onset of voltage under perfect-coupling conditions occurs when $I_p = \pm(I_{pc} + I_{sc})$, as is seen from Eq. (3.36). The value of I_p at which decoupling occurs is, from Eqs. (3.21), (3.22), and (3.35),

$$I_{pd}^{\pm\pm} = \pm(I_{pc} + I_{sc}) \pm (I_0 - I_{sc}) \times [1 + R_p^{-1}(R_L^{-1} + R_s^{-1})^{-1}] . \tag{3.38}$$

Similarly, from Eqs. (3.21) and (3.35) we obtain the voltage at decoupling,

$$V_{\pm\pm} = \pm(I_0 - I_{sc})(R_s^{-1} + R_L^{-1})^{-1} , \tag{3.39}$$

where in the above two equations the upper (lower)

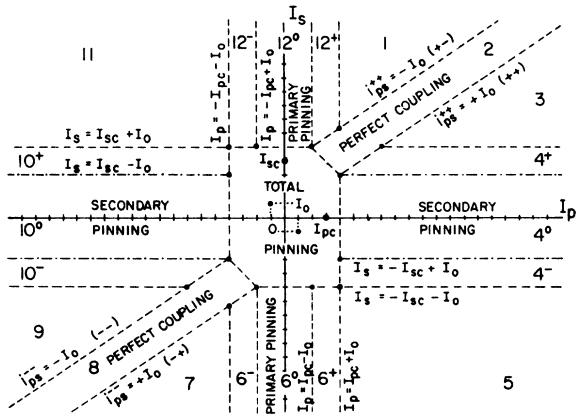

FIG. 8. $I_p - I_s$ map for magnetically coupled films with relatively strong pinning and parameters in the ratios $I_{pc}:I_{sc}:I_0 = 3:4:1$ and $R_p:R_s = 2:3$. The behavior of the current-voltage characteristics in each numbered region is summarized in Table I.

signs hold when the voltage and the primary current at decoupling are positive (negative).

The time-averaged power dissipated in the primary, the secondary, and the load is, in general,

$$P_p = I_{pc}\langle |V_p| \rangle + \langle V_p^2/R_p \rangle , \tag{3.40}$$

$$P_s = I_{sc}\langle |V_s| \rangle + \langle V_s^2/R_s \rangle , \tag{3.41}$$

$$P_L = \langle V_s^2/R_L \rangle , \tag{3.42}$$

where the brackets denote time averages. The first term on the right-hand side of Eqs. (3.40) and (3.41) represents power dissipated locally at pinning sites; the second term represents power dissipated via viscous losses almost uniformly between pinning sites. The sum of P_p, P_s, and P_L is, of course, equal to the time-averaged power input to the primary, $P_{in} = \langle I_p V_p \rangle$.

The power delivered to the load, $P_L = \langle V_s^2/R_L \rangle$, is greatest at the decoupling condition, where $V_s = V_{\pm\pm}$. With the help of Eq. (3.39) we find that the maximum power delivered to the load, obtained when $R_L = R_s$, is

$$P_{L\,\max} = \tfrac{1}{4}(I_0 - I_{sc})^2 R_s . \tag{3.43}$$

With further use of Eqs. (3.38) and (3.39), we find that the transfer efficiency of the device is then

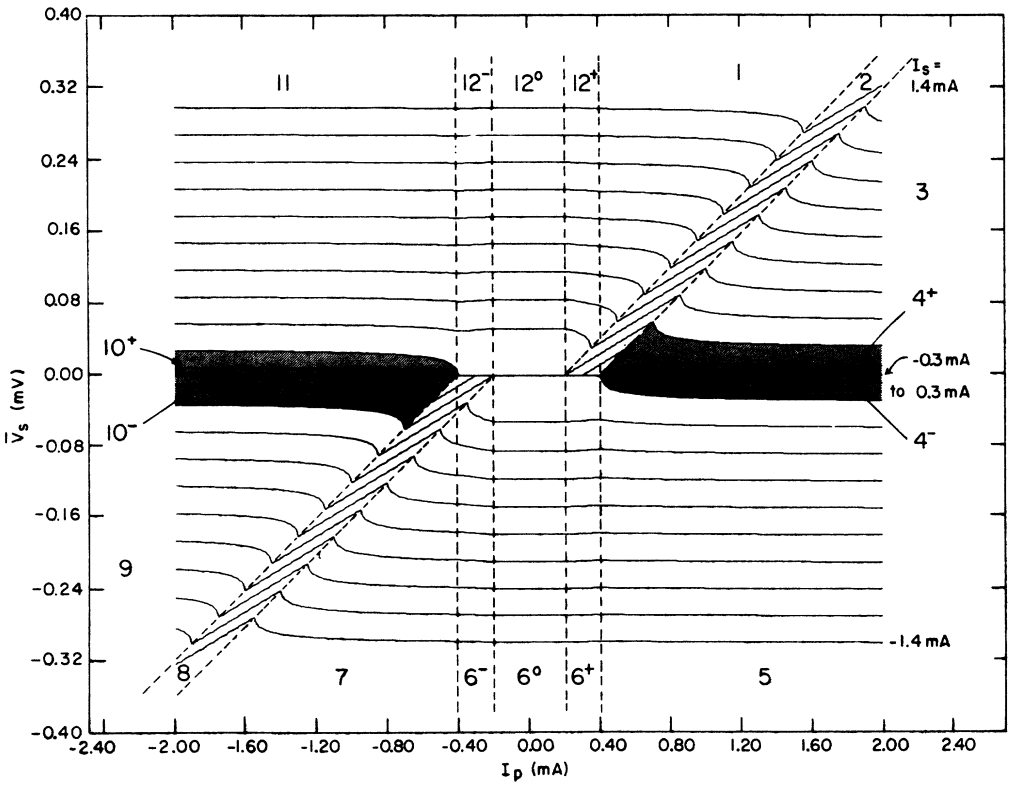

FIG. 9. Theoretical time-averaged secondary voltage $\bar{V}_s$ vs primary current I_p, calculated as described in the text for secondary currents $I_s = -1.4, -1.3, \ldots, 1.3, 1.4$ mA. Model parameters $I_{pc} = 0.3$ mA, $I_{sc} = 0.4$ mA, $I_0 = 0.1$ mA, $R_p = 0.2\ \Omega$, and $R_s = 0.3\ \Omega$ were selected to describe strongly pinned magnetically coupled films. Numbered regions correspond to those of the $I_p - I_s$ map of Fig. 8.

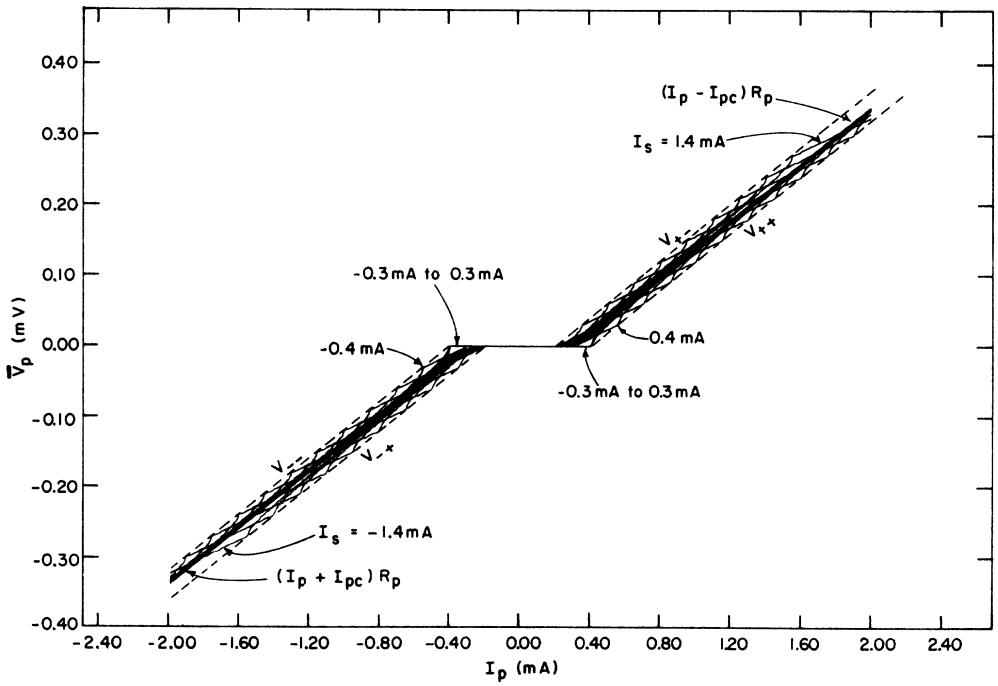

FIG. 10. Theoretical time-averaged primary voltage $\bar{V}_p$ vs primary current I_p, calculated as described in the text for secondary currents $I_s = -1.4, -1.3, \ldots, 1.3, 1.4$ mA. Model parameters are those used for Fig. 9. The four dashed lines illustrate the decoupling voltages $V_{\pm\pm} = (I_p \mp I_{pc} \mp I_0)R_p$ [Eq. (3.21) of the text]. Note also that, for primary currents well above the decoupling current, $\bar{V}_p$ asymptotically approaches $(I_p - I_{pc})R_p$, regardless of the value of I_s.

$$P_{L\,\max}/P_{\text{in}} = \tfrac{1}{2}[1 + R_s/2R_p + (I_{pc} + I_{sc})/(I_0 - I_{sc})]^{-1}\,, \tag{3.44}$$

where $P_{in} = I_{pd}^{\pm\pm} V_{\pm\pm}$ is the power delivered to the primary. Thus at least as much power is dissipated in the transformer as is delivered to the load under these conditions.

The transfer efficiency of the transformer can be improved by reducing the load resistance, but at the expense of the power delivered to the load. When $R_L \ll R_s$ or R_p, the transfer efficiency becomes

$$P_L/P_{\text{in}} \approx -I_{s++}/I_{p++} = \frac{I_0 - I_{sc}}{I_0 + I_{pc}}\,, \tag{3.45}$$

which approaches unity in the limit of very weak pinning, but the load power then becomes

$$P_L \approx (I_0 - I_{sc})^2 R_L \ll P_{L\,\max}\,. \tag{3.46}$$

IV. DISCUSSION

The above treatment describes well, we believe, the essential features of the behavior of magnetically coupled superconducting films. We discussed in Sec. II the periodic coupling energy and how this yields a periodic coupling force whose maximum value is very nearly isotropic. We then examined in Sec. II the equations of motion and found that the important features in the current-voltage characteristics are determined by only five parameters. Of these five, the most interesting from the present point of view is I_0, which is proportional to the maximum coupling force, discussed in Sec. II.

A theory based upon the London model of the dependence of I_0 upon the magnetic field B and the specimen parameters d_p, d_s, d_i, λ_p, and λ_s will be presented in a subsequent paper.[4] Within this theory, the temperature dependence of I_0 enters via that of λ_p and λ_s. Experimental results should soon reveal how successfully the London model can account for the details of the behavior of I_0.

Some of the results of the present paper (in particular, the current-voltage characteristics in regions of partial decoupling) depend upon the simplifying assumption of a sinusoidal coupling force, Eq. (3.13). Since this assumption is justified only when the one-reciprocal-lattice-vector approximation holds and when slippage occurs parallel to a lattice vector, a more general treatment to include more realistic coupling forces would be desirable. Such a generalization is straightforward, although computations of the current-voltage characteristics would be more time consuming because of the numerical integrations required.

For simplicity, in this paper we have ignored edge effects. If flux pinning in coupled films is not

essentially homogeneous throughout the bulk, but is most pronounced at the specimen edges, as is the case for edge pinning,[9] then our equations of motion will need important revisions. Moreover, there remains the unanswered question of the details of the primary-secondary-fluxoid interaction near the specimen edges, where fluxoids are nucleating or annihilating. Such edge effects probably will have to be included in a description of coupling between thin superconducting strips of narrow width.

Another subject for future investigation is the behavior of coupled films in the presence of high-frequency oscillatory components of the primary and secondary currents. Such components may well produce structure in $\overline{V}_p$ and $\overline{V}_s$ when the period of oscillation is close to an integer multiple of the natural period τ of slippage between the primary and secondary lattices.

ACKNOWLEDGMENTS

Thanks are extended to John T. Seeman for carrying out the numerical computations reported in this paper, to Dr. Rudolf P. Huebener for his hospitality at Argonne National Laboratory and for encouragement during the early stages of this work, to Dr. Bernard Serin for helpful advice, and to Dr. John W. Ekin for his close collaboration during the final stages of this work.

[1]I. Giaever, Phys. Rev. Lett. 15, 825 (1966); Phys. Rev. Lett. 16, 460 (1966).
[2]P. E. Cladis, R. D. Parks, and J. M. Daniels, Phys. Rev. Lett. 21, 1521 (1968).
[3]J. W. Ekin, B. Serin, and J. R. Clem, following paper, Phys. Rev. B 9, 912 (1974).
[4]J. R. Clem (unpublished).
[5]F. London, *Superfluids I, Macroscopic Theory of Superconductivity* (Dover, New York, 1961), Sec. 3, p. 29.
[6]J. Pearl, J. Appl. Phys. 37, 4139 (1966).
[7]M. D. Sherrill, Phys. Rev. B 7, 1908 (1973).
[8]For a good discussion and review of flux flow, see Y. B. Kim and M. J. Stephen, in *Superconductivity*, edited by R. D. Parks (Marcel Dekker, New York, 1969), Vol. II, Chap. 19, p. 1107.
[9]J. R. Clem, R. P. Huebener, and D. E. Gallus, J. Low Temp. Phys. 12, 449 (1973).

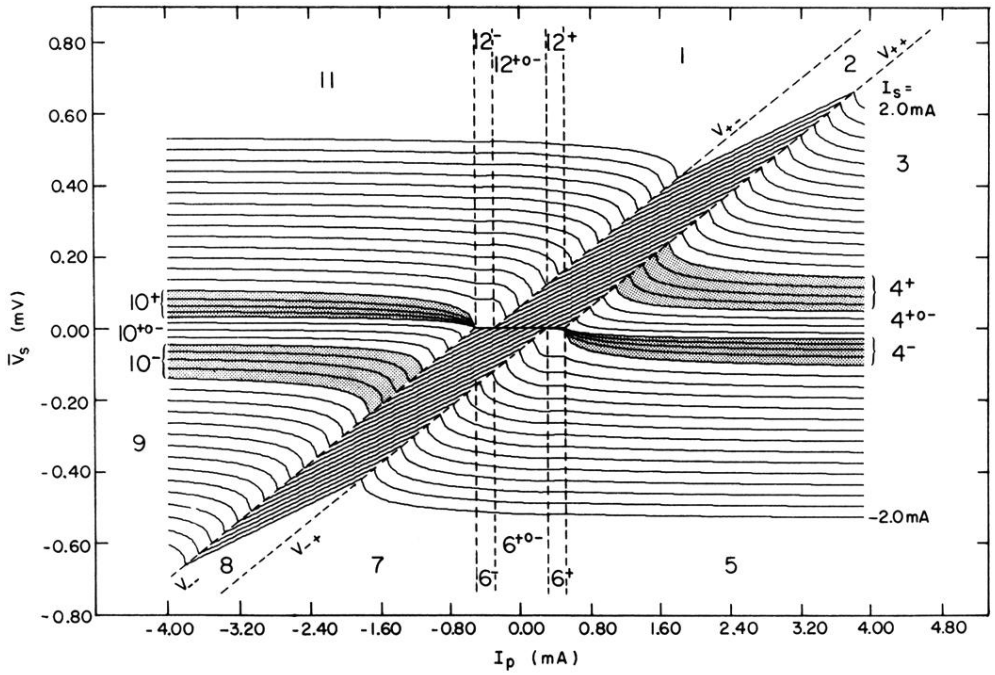

FIG. 6. Theoretical time-averaged secondary voltage $\bar{V}_s$ vs primary current I_p, calculated as described in the text for secondary currents $I_s = -2.0, -1.9, \ldots, 1.9, 2.0$ mA. Model parameters $I_{pc} = 0.1$ mA, $I_{sc} = 0.2$ mA, $I_0 = 0.4$ mA, $R_p = 0.2\ \Omega$, and $R_s = 0.3\ \Omega$ were selected to describe weakly pinned magnetically coupled films. Numbered regions correspond to those of the $I_p - I_s$ map of Fig. 3.

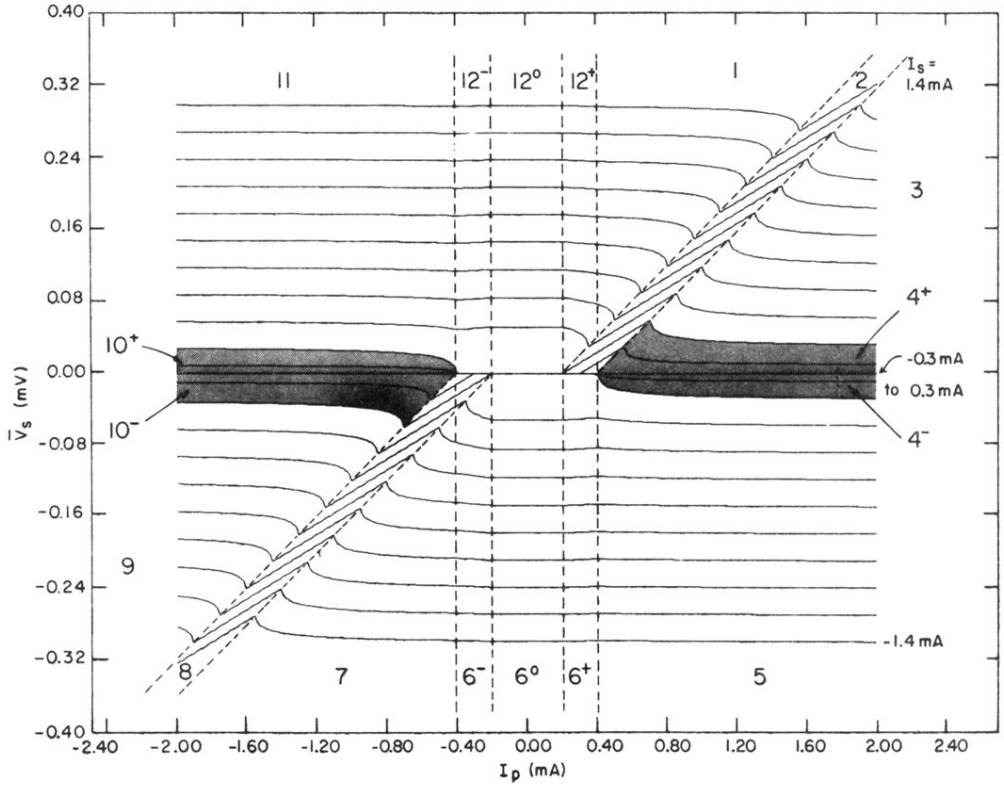

FIG. 9. Theoretical time-averaged secondary voltage $\bar{V}_s$ vs primary current I_p, calculated as described in the text for secondary currents $I_s = -1.4, -1.3, \ldots, 1.3, 1.4$ mA. Model parameters $I_{pc} = 0.3$ mA, $I_{sc} = 0.4$ mA, $I_0 = 0.1$ mA, $R_p = 0.2\ \Omega$, and $R_s = 0.3\ \Omega$ were selected to describe strongly pinned magnetically coupled films. Numbered regions correspond to those of the $I_p - I_s$ map of Fig. 8.